Letters

Peak Operation Mode-Matching Online Fast Frequency Response Capacity Estimation for Lithium-ion Battery Energy Storage System

Shaoxin Shi, Qiao Peng, *Member, IEEE*, Tianqi Liu, *Senior Member, IEEE*, and Jinhao Meng, *Senior Member, IEEE*

***Abstract*—Fast frequency response capacity (FFRC) is critical for frequency support performance and safe operation of battery energy storage system (BESS). Conventional methods fail to match the specific fast frequency response (FFR) requirements of the grid, leading to conservative assessment or inaccurate estimation-caused penalty. This letter proposes a peak operation mode (POM)-matching online FFRC estimation method for BESSs. An elastic resistor-based equivalent circuit model is developed to address modeling inaccuracy under strongly nonlinear impedance behavior during FFR-POM. Then, an impedance construction method is developed to obtain the continuous impedance curve, based on which online FFRC estimation is realized by iterative searching under multiconstraint. Experimental results prove the excellent estimation accuracy of the proposed method under various conditions.**

***Index Terms*—Equivalent circuit model (ECM), fast frequency response capacity (FFRC), lithium-ion battery energy storage system (BESS), online estimation, peak operation mode (POM).**

I. Introduction

LITHIUM-ION battery energy storage systems (BESSs) are one of the key technologies in modern power systems due to the rapid response speed and high controllability [1]. Among different ancillary services required by the grid, fast frequency response (FFR) is critical for BESSs [2]. To maximize efficiency and ensure battery safety, accurate evaluation of available FFR capacity (FFRC) is important.

The FFRC of BESS is constrained by both the power conversion system and the battery output capacity. The power conversion system constraint has been widely discussed [3], while the limitations on the battery have rarely been reported. Such output capacity of BESS is usually referred to as the state of power (SOP). When assessing the SOP of BESS, most existing studies assume a fixed peak operation mode (POM) within the prediction window, e.g., constant current (CC), constant voltage, or constant power [4]. However, the output power of BESS under FFR-POM differs a lot from the conventional POMs, as depicted in Fig. 1. Note that the polarization effects, especially the electrochemical polarization and concentration polarization of battery, are significantly impacted by the POM, i.e., the time-varying current trajectory [4]. Thus, existing methods designed for conventional POMs are not applicable for FFRC estimation, which will lead to conservative results or induce safety issues. In [5], the concept of sustaining power boundary is proposed for assessing the inertia-supporting capacity of BESS, reducing the estimation error by 50% over the CC-POM. These findings highlight the importance of customizing POM for estimating BESS's output capacity. When estimating the FFRC of BESS, the specific FFR-POM that typically consists of activation phase and sustaining support phase should be adequately considered [6], which has not been discussed in previous studies.

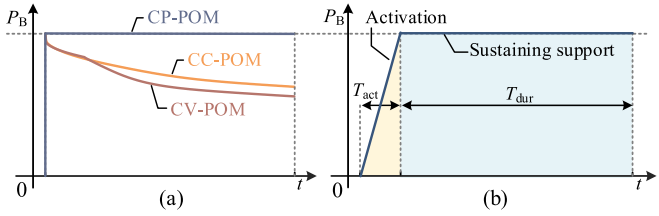

Fig. 1. Output power of BESS under: (a) Convention POMs and (b) FFR-FOM, where P_B is the output power, T_{act} is the activation time, and T_{dur} is the sustaining support time.

For SOP estimation, the model-based methods are widely utilized, which can capture the impedance of battery and support online application [7], [8]. Equivalent circuit models (ECMs), such as the Thevenin and dual-polarization (DP) models, are common options due to the tradeoff between accuracy and computational cost. However, these models can hardly capture the nonlinear behaviors of battery during unconventional POM [9], where the high rates and sustaining output demand may significantly intensify polarization [10]. Although electrochemical

Received 14 May 2025; revised 20 June 2025 and 12 July 2025; accepted 23 July 2025. Date of publication 1 August 2025; date of current version 8 September 2025. This work was supported by the National Natural Science Foundation of China under Grant 52207218 and in part by the Guizhou Provincial Science and Technology Support Plan under Grant [2023] General 293. *(Corresponding author: Qiao Peng.)*

Shaoxin Shi, Qiao Peng, and Tianqi Liu are with the College of Electrical Engineering, Sichuan University, Chengdu 610065, China (e-mail: shishaoxin@stu.scu.edu.cn; qpeng@scu.edu.cn; tqliu@scu.edu.cn).

Jinhao Meng is with the National Innovation Platform (Center) for Industry-Education Integration of Energy Storage Technology, Xi'an Jiaotong University, Xi'an 710049, China, and also with the the School of Electrical Engineering, Xi'an Jiaotong University, Xi'an 710049, China (e-mail: jinhao@xjtu.edu.cn).

Color versions of one or more figures in this article are available at https://doi.org/10.1109/TPEL.2025.3594960.

Digital Object Identifier 10.1109/TPEL.2025.3594960

model (EM) can characterize these phenomena, the numerous parameters and partial differential equations of EM impose a huge computational burden, limiting its online application. Aiming at this point, several studies consider electrochemical effects in ECMs. For example, Arrhenius and Butler-Volmer equations are introduced into the Thevenin model in [11] to reflect current-rate-dependent polarization. The dependence relationships of current and concentration are incorporated in [12]. However, these models suffer from complex parameterization and high computational burden and fail to capture complex polarization under time-varying POM. As revealed in [13], the negative resistor can be applied to address the intensive polarization effect of battery in irregular working conditions, while its applicability in FFRC estimation has not been investigated. Therefore, there still lacks effective methods regarding battery modeling under FFR-POM for FFRC estimation.

In view of the above issues, a novel model-based method for POM-matching online FFRC estimation is proposed in this letter, where an elastic resistor-based ECM (ER-ECM) is applied. The main contributions are summarized as follows.

1) ER-ECM is developed for accurately capturing the nonlinear characteristics of battery with a simple structure.
2) The developed experiment-based full-range impedance construction method efficiently supports online application of the ER-ECM.
3) The proposed iterative searching-based multiconstraint FFRC estimation strategy improves accuracy and safety of battery.

II. FFRC Online Estimation Method

A. FFR Output Requirements

FFR is rapidly adjusting the output power to compensate for the grid power deficit and prevent frequency drop. For central dispatching and revenue settlement, the FFR-POM is specified by grid operators. The output power of BESS should match the POM requirement, or the FFR support cannot be certificated and rewarded. Typically, the FFR consists of two stages, i.e., activation and sustaining support [2], as shown in Fig. 1(b). The FFR output power can be described as

$$P_{\mathrm{B}}(t)=\begin{cases}P_{\mathrm{B,max}}\frac{t}{T_{\mathrm{act}}}, 0\le t\le T_{\mathrm{act}}\\ P_{\mathrm{B,max}}, t>T_{\mathrm{act}}.\end{cases} \tag{1}$$

B. ER-ECM

In this letter, a representative cell model is employed to approximate the BESS behavior, assuming great consistency among battery cells. The consistency of cells can be maintained by improved manufacturing and equalization technologies and has been validated in prior studies [14], [15].

Under the FFR-POM, battery's current and voltage exhibit monotonically grow and decline with mutual coupling. Impacted by a sustaining and high discharge rates output condition, the complex effects from solid phase diffusion reaction and lithium depletion in the electrolyte accelerate the nonlinearity of battery impedance at the late stage [16]. Moreover, experimental results indicate that the nonlinearity is highly related to real-time state of charge (SOC) of battery. It is difficult for conventional ECMs to describe the nonlinearity, as their component parameters are positive and fixed, which are typically identified in normal conditions.

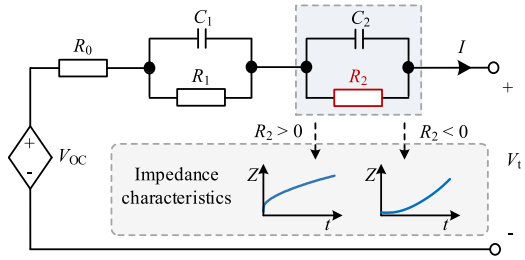

Fig. 2. Model structure of ER-ECM.

Thus, an elastic resistor-based *RC* link is proposed in this paper to capture the complex polarization of battery, based on which the ER-ECM is developed. The structure of ER-ECM is shown in Fig. 2, where R_2 is the elastic resistor. As shown in Fig. 2, R_2 can be positive or negative, and its corresponding *RC* link characterizes the phenomenon of polarization saturation or enhancement, respectively. The elastic resistor-based *RC* link is characterizing the combined effect of solid phase diffusion reaction and lithium depletion in the electrolyte of battery. Note that the ER-ECM is different from the conventional DP model, as the second *RC* link represents different electrochemical reactions within the battery, and with R_2 can be negative. The operational characteristics of a battery based on the ER-ECM are expressed as

$$\begin{cases}V_{\mathrm{p}i,k}=V_{\mathrm{p}i,k-1}e^{-T_{\mathrm{s}}/\tau_i}+I_{k-1}R_i(1-e^{-T_{\mathrm{s}}/\tau_i})\\ V_{\mathrm{t},k}=V_{\mathrm{OC},k}-V_{\mathrm{p1},k}-V_{\mathrm{p2},k}-I_kR_0\\ \mathrm{SOC}_k=\mathrm{SOC}_{k-1}-I_{k-1}T_{\mathrm{s}}/Q_{\mathrm{N}}\end{cases} \tag{2}$$

where the subscript k denotes the time step, T_{s} denotes the sampling interval, $V_{\mathrm{p}i}$ $(i=12)$ and $\tau_i=R_iC_i$ are the voltage and time constants of the ith *RC* link, respectively, V_{t} and I are the terminal voltage and current, respectively, R_0 is the ohmic resistance, Q_{N} is the nominal capacity, and V_{OC} is the open circuit voltage, which can be obtained by the SOC [17].

The equivalent impedance of ER-ECM Z_{eq} is derived as

$$Z_{\mathrm{eq}}(t)=R_0+\underbrace{R_1(1-e^{-t/R_1C_1})+R_2(1-e^{-t/R_2C_2})}_{Z_{\mathrm{p}}(t)} \tag{3}$$

where Z_{p} is the polarization impedance, $R_2\neq 0$, and $C_2>0$.

C. Full-Range Impedance Construction

As the elastic resistor can be positive or negative, the parameter identification of the ER-ECM is challenging, especially in online application. Conventional identification is performed under normal operating conditions with relatively mild discharge rates, which lacks information on nonlinear polarization behavior under FFR, leading to model mismatches. In this letter, the experiment-based impedance measurement and impedance curve fitting method is applied to obtain the full-range impedance curve for online parameter identification. At

the experiment stage, the model parameters are identified under the predesigned FFR pulses (FFRPs) test, consisting of pulses at varying T_{act} and a fixed T_{dur} for 30 s, covering SOCs from 80% to 20% at 10% intervals. Prior to each test, the battery is discharged to the specified SOC and fully relaxed, then discharged under the FFR pulses until the voltage reaches its cutoff, recording the equivalent impedance corresponding to the FFR pulses.

Based on the experimental impedance, the model parameters can be identified offline, and the relationship of model variation with SOC can be established for online application. Conventional parameter fitting (PF) method relating parameters to SOC may cause overfitting when R_2 crosses zero for ER-ECM. Considering the continuous variation of the impedance curve, a hybrid strategy is proposed to identify the impedance, where the PF is applied to R_0 and curve fitting is performed for Z_{p} under different SOC and T_{act}, i.e.,

$$Z_{\mathrm{p}}(t) = f(\mathrm{SOC}, T_{\mathrm{act}}, t). \tag{4}$$

The full range of polarization impedance curves can be constructed by (4), which avoids overfitting of R_2.

Based on (4), the time-dependent curve of $Z_{\mathrm{p},k}(t)$ can be estimated online by real-time T_{act} and estimated SOC_k. Then, the ER-ECM parameters $\psi = [R_1,\ C_1,\ R_2,\ C_2]$ of $Z_{\mathrm{p},k}(t)$ are identified using a multistart nonlinear least squares by minimizing

$$\min_{\psi} F(\psi) = \sum_{t\in\mathbb{R}} \left[Z_{\mathrm{p},k}(t) - \hat{Z}_{\mathrm{p},k}(t,\psi)\right]^2 \tag{5}$$

where $\hat{Z}_{\mathrm{p}}$ is the estimated polarization impedance.

D. Multiconstraint FFRC Estimation

With the identified ER-ECM parameters, the FFRC can be estimated. To ensure safe operation, FFRC estimation must consider the constraints of voltage, current, SOC, and state of energy (SOE). Since the estimation target is output power, the FFRC under SOE constraint at moment k can be directly expressed as

$$P^{\mathrm{SOE}}_{\mathrm{B,max},k} = \frac{(\mathrm{SOE}_k - \mathrm{SOE}_{\min})E_{\mathrm{N}}}{(T_{\mathrm{sup}} + T_{\mathrm{act}}/2)} \tag{6}$$

where E_{N} is the nominal energy and $\mathrm{SOE}_{\min}$ is the lower limit of SOE.

Unlike SOE, voltage, current, and SOC are time-varying and couple with each other under FFR-POM. At the same time, given the low cost and fast computation requirements for online deployment. An iterative searching strategy is proposed in this letter to address these constraints and online requirements. The BESS output power over the prediction window is

$$\begin{aligned} P_{\mathrm{B},k+j} = I_{k+j}[&h_1(\mathrm{SOC}_{k+j-1}, I_{k+j-1}) \\ &- h_2(V_{\mathrm{p}i,k+j-1}, I_{k+j-1}) - R_{0,k} I_{k+j}] \end{aligned} \tag{7}$$

where $j = \{1,\ \ldots,\ K\}$ with K being the prediction window length, $P_{\mathrm{B},k+j}$ denotes the discrete FFR power at time k+j, with $P_{\mathrm{B},k+j} = jT_{\mathrm{s}}P_{\mathrm{B,max},k}/T_{\mathrm{act}}$ during the activation stage, and $P_{\mathrm{B},k+j} = P_{\mathrm{B,max},k}$ during the duration stage, h_1 represents V_{OC} as a function of the SOC and I at the previous moment, and h_2 expresses $V_{\mathrm{p}i}$ as a function of polarization voltage and I at the historical moment.

Fig. 3. Experimental setup platform.

Solving (7) yields the estimated I_{k+j}, and then V_{k+j} and SOC_{k+j}. This chainwise estimation continues iteratively until the end of a prediction window. Due to the monotonic evolution of battery current, voltage, and SOC, all their boundary conditions occur at end step K, which is denoted as $Y_K = [V_K,\ I_K,\ \mathrm{SOC}_K]$. The constraint vector of Y_K is denoted as $Y_{\mathrm{c}} = [V_{\mathrm{t,min}},\ I_{\max},\ \mathrm{SOC}_{\min}]$, corresponding to the cutoff voltage, the maximum current, and the lower limit of SOC, respectively. Then, based on the relationship between Y_K and Y_{c}, the estimated $P_{\mathrm{B,max}}$ can be iteratively adjusted according to the following until multiconstraints are satisfied:

$$\begin{cases} Y^n_{k+K} = g(P^n_{\mathrm{B,max},k}) \\ P^n_{\mathrm{B,max},k} = P^{n-1}_{\mathrm{B,max},k} + w^{n-1}_k P_{\mathrm{d}} \end{cases} \tag{8}$$

where n is the iteration count, $g(.)$ denotes an implicit nonlinear function of a given $P_{\mathrm{B,max}}$ with estimate Y_K, P_{d} is the adjustment step, and w is the correction weight, which is used to adjust the direction of the next search, and w is determined as follows.

1) All the variables in Y_K are within the constraint, indicating that $P_{\mathrm{B,max}}$ is underestimated. Set $w = 1$.
2) Any variables in Y_K violate the constraint, indicating that $P_{\mathrm{B,max}}$ is overestimated. Set $w = -1$.
3) Some variables in Y_K opportunely reach their thresholds while others still satisfy their constraints, indicating that $P_{\mathrm{B,max}}$ is optimal. Set $w = 0$, and the iteration is terminated.

To balance estimation efficiency and accuracy, the variable in Y_K approaches its threshold with absolute deviation of less than 0.4% can be considered as reaching the threshold. Considering the continuous variation of the battery output capacity, the estimation result at moment k-1 is used as the initialization of the iteration at moment k, i.e., $P^1_{\mathrm{B,max},k} = P_{\mathrm{B,max},k\text{-}1}$. Therefore, the multiconstraint FFRC estimation result is obtained by

$$P^{\mathrm{MC}}_{\mathrm{B,max},k} = \min(P^{\mathrm{SOE}}_{\mathrm{B,max},k}, P_{\mathrm{B,max},k}). \tag{9}$$

III. Experimental Validation

A. Experimental Setup

The experimental tests are conducted on a cylindrical ICR-18650 lithium-ion battery with nominal capacity of 1.5 Ah and rated voltage of 3.6 V. The operating constraints are $[V_{\mathrm{t,min}},\ I_{\max},\ \mathrm{SOC}_{\min},\ \mathrm{SOE}_{\min}]$ = [2.5 V, 27 A, 15%, 15%]. The battery test platform shown in Fig. 3 consists of a programmable battery charge/discharge tester, a host computer for generating

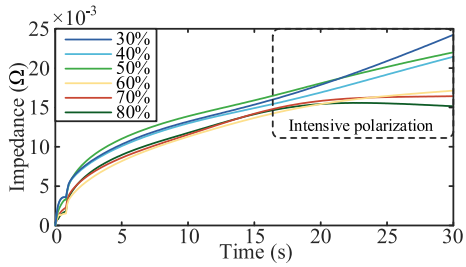

Fig. 4. Polarization impedance results for $T_{\rm act} = 1$ s FFRP test.

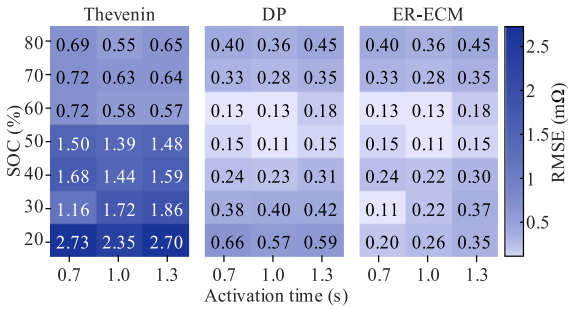

Fig. 5. RMSE of different models in FFRP test.

control signals and collecting data, and a temperature chamber for ambient control. The time configuration of the FFR-POM is $[T_{\rm act}, T_{\rm dur}] = [\ 0.7/1/1.3$ s, 30 s] with reference to Energinet's FFR technical requirements in the Nordic Synchronous Area [2]. $P_{\rm d}$ is set to 0.1 W.

B. Validation of ER-ECM

This section verifies the accuracy of the proposed ER-ECM. Fig. 4 presents the polarization impedance under the $T_{\rm act} = 1$ s FFRP test. The results reveal a distorted saturation growth in the high SOC region and a pronounced acceleration in the low SOC region, indicating strong nonlinear polarization behavior. The ER-ECM is then compared with the Thevenin and DP models. As shown in Fig. 5, the ER-ECM consistently outperforms the others across the full SOC range, achieving a maximum root-mean-square error (RMSE) of 0.45 mΩ, which is 83% and 33% less than the Thevenin and DP models, respectively.

C. Validation of FFRC Estimation

The proposed FFRC estimation method is validated through static and dynamic tests. Given a set of SOC points with an interval of 0.1% in the range of 20% –80% SOC, the proposed method will produce the FFRC estimation of the battery under the equilibrium initial state. In addition, online SOE estimation is realized by leveraging the strong correlation between SOC and SOE [18]. Its validity is verified via static FFRC tests conducted at SOC levels from 25% to 75% in 10% intervals. In each test, an FFR pulse is injected into a fully rested battery at the specified SOC. When the injected FFR pulse did not reach boundary conditions, the amplitude of the pulse is adjusted until a reference value that meets the boundary conditions is obtained.

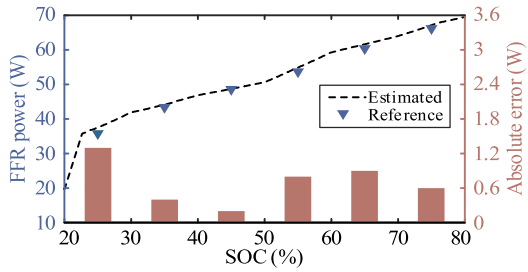

Fig. 6. Experimental results of static $T_{\rm act} = 1$ s FFRC estimation.

TABLE I
ESTIMATION ERROR OF STATIC FFRC (%)

Method	RMSE	MAE
Proposed	1.95	1.63
HPPC&DP	9.1	7.69
PF&DP	6.38	4.48

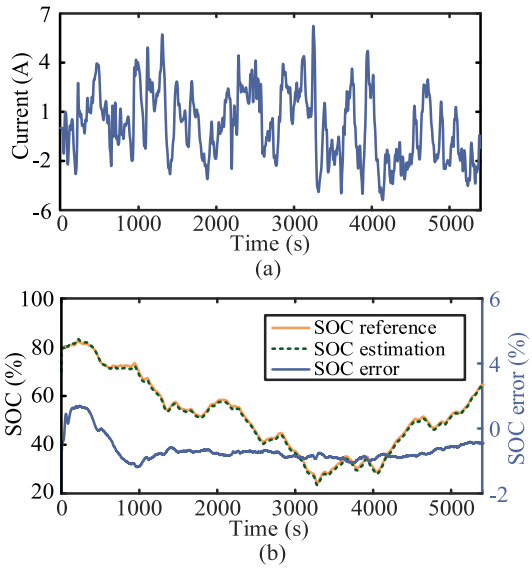

Fig. 7. FRWC current profile and SOC estimation results. (a) Current. (b) Online SOC estimation results.

Fig. 6 shows the results of static $T_{\rm act} = 1$ s FFRC estimation. The estimated FFRC accurately tracks the reference values with a maximum absolute error of 1.3 W, which indicates the excellent performance of the proposed method. A comparison between the proposed method and two methods based on the hybrid power pulse characterization (HPPC) and PF parameterized DP model is given in Table I. The HPPC method yields RMSE and mean absolute error (MAE) of 9.1% and 7.69%, respectively, while the PF method results in errors of 6.38% and 4.48% . In contrast, the proposed method achieves lowest RMSE and MAE of 1.95% and 1.63% . It represents a reduction in RMSE by 7.15% and 4.43% compared to HPPC and PF methods, respectively.

Dynamic FFRC tests are conducted under frequency regulation working condition (FRWC) with an interval of 1000 s, as shown in Fig. 7(a). The dynamic FFRC test follows the same principle as the static one but without a relaxation period before the FFR pulse. An extended Kalman filter algorithm is employed

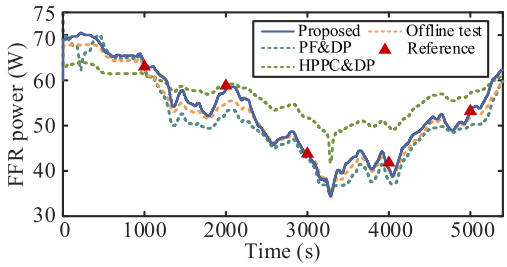

Fig. 8. Validation of dynamic $T_{\mathrm{act}} = 1$ s FFRC estimation under FRWC profile.

TABLE II
ESTIMATION ERROR OF DYNAMIC FFRC BY DIFFERENT METHODS (%)

Method	RMSE	MAE
Proposed	4.22	3.04
Offline test	5.49	4.0
HPPC&DP	10.91	8.06
PF&DP	11.26	8.84

for online SOC estimation, achieving high accuracy with the estimation error consistently within 2%, as shown in Fig. 7(b). Based on the online SOC and SOE estimation results, the FFRC estimation under FRWC can be realized.

Fig. 8 illustrates the dynamic $T_{\mathrm{act}} = 1$ s FFRC estimation results, comparing the proposed method with the offline test, HPPC, and PF methods. The offline test method measures the FFRC under various SOC and T_{act} in a controlled experimental environment. It assumes that the measured FFRC changes continuously and monotonically with SOC, and this trend is captured using a fitting function. Since the procedure of the offline test is same as the static FFRC test, the measurement results of the offline test are based on the static FFRC test results. The proposed method accurately tracks the reference throughout the test, while the offline test exhibited a noticeable deviation around 2000 s, indicating its limitation for online applications. Furthermore, both the HPPC and PF methods demonstrate inferior performance. As summarized in Table II, the proposed method achieves the highest accuracy, with both RMSE and MAE below 4.3% . Compared with the offline test, HPPC, and PF methods, the RMSE of the proposed method is reduced by 1.27%, 6.69%, and 7.04%, respectively.

IV. CONCLUSION

This letter proposes a novel POM-matching online FFRC estimation method for BESS. The ER-ECM can effectively capture the strong nonlinearity of battery polarization with a simple structure. An experiment-based impedance construction method facilitates reliable online application of the ER-ECM. Moreover, the multiconstraint FFRC estimation strategy improves estimation accuracy and ensures safety of battery. Experimental tests validate the proposed method, which realizes reliable online FFRC estimation with a MAE below 3.1% under different operating conditions.

This study focuses on battery modeling and online FFRC estimation under FFR-POM, with an assumption that the consistency among battery cells in BESS remains within good limits. When the inconsistency of cells increases, expansion and integration of cells' models may be required, which will be explored in future work. Moreover, the adaptability of the proposed method on different types of battery and under different grid support conditions will be investigated. The operational limitations of the power conversion system will be comprehensively considered as well.

REFERENCES

[1] C. Zhao, P. B. Andersen, C. Træholt, and S. Hashemi, "Grid-connected battery energy storage system: A review on application and integration," *Renew. Sustain. Energy Rev.*, vol. 182, Aug. 2023, Art. no. 113400.
[2] Z. Hameed, C. Traeholt, and S. Hashemi, "Investigating the participation of battery energy storage systems in the Nordic ancillary services markets from a business perspective," *J. Energy Storage*, vol. 58, Feb. 2023, Art. no. 106464.
[3] H. S. Das, S. Li, B. Lu, J. Wang, S. Rahman, and X. Fu, "Exploring dynamic P-Q capability and abnormal operations of inverter-based resources," *IEEE J. Emerg. Sel. Top. Power Electron.*, vol. 12, no. 2, pp. 1608–1618, Apr. 2024.
[4] R. Guo, C. Hu, and W. Shen, "Battery peak power assessment under various operational scenarios: A comparative study," *IEEE Trans. Transp. Electrific.*, vol. 11, no. 1, pp. 2489–2503, Feb. 2025.
[5] T. Liu, Y. Dai, Q. Peng, X. Zeng, G. Chen, and J. Meng, "Inertia emulation-oriented evaluation method of sustaining power boundary for lithium-ion battery energy storage system," *IEEE Trans. Energy Convers.*, vol. 39, no. 4, pp. 2362–2376, Dec. 2024.
[6] L. Meng et al., "Fast frequency response from energy storage systems—A review of grid standards, projects and technical issues," *IEEE Trans. Smart Grid*, vol. 11, no. 2, pp. 1566–1581, Mar. 2020.
[7] X. Shen et al., "State of power estimation for LIBs in electric vehicles: Recent progress, challenges, and prospects," *J. Energy Storage*, vol. 115, Apr. 2025, Art. no. 116042.
[8] R. Zhang, K. Wang, Z. Yu, and G. Zhao, "A novel method for estimating State of power of lithium-ion batteries considering core temperature," *Batteries*, vol. 10, no. 12, Dec. 2024, Art. no. 12.
[9] R. Guo and W. Shen, "Recent advancements in battery state of power estimation technology: A comprehensive overview and error source analysis," *J. Energy Storage*, vol. 103, Dec. 2024, Art. no. 114294.
[10] M. J. Lain and E. Kendrick, "Understanding the limitations of lithium ion batteries at high rates," *J. Power Sources*, vol. 493, May 2021, Art. no. 229690.
[11] A. Chen, W. Zhang, C. Zhang, W. Huang, and S. Liu, "A temperature and current rate adaptive model for high-power lithium-titanate batteries used in electric vehicles," *IEEE Trans. Ind. Electron.*, vol. 67, no. 11, pp. 9492–9502, Nov. 2020.
[12] X. Zhao et al., "A modified high C-rate battery equivalent circuit model based on current dependence and concentration modification," *Electrochimica Acta*, vol. 478, Feb. 2024, Art. no. 143833.
[13] Y. Dai, Q. Peng, T. Liu, J. Meng, F. Gao, and F. Blaabjerg, "Negative resistor-based equivalent circuit model of lithium-ion battery energy storage system for grid inertia support," *IEEE Trans. Power Electron.*, vol. 39, no. 11, pp. 15217–15230, Nov. 2024.
[14] Z. Zhou, Y. Kang, Y. Shang, N. Cui, C. Zhang, and B. Duan, "Peak power prediction for series-connected LiNCM battery pack based on representative cells," *J. Clean. Prod.*, vol. 230, pp. 1061–1073, Sep. 2019.
[15] J. Tian, Y. Fan, T. Pan, X. Zhang, J. Yin, and Q. Zhang, "A critical review on inconsistency mechanism, evaluation methods and improvement measures for lithium-ion battery energy storage systems," *Renew. Sustain. Energy Rev.*, vol. 189, Jan. 2024, Art. no. 113978.
[16] A. Goshtasbi, R. Zhao, R. Wang, S. Han, W. Ma, and J. Neubauer, "Enhanced equivalent circuit model for high current discharge of lithium-ion batteries with application to electric vertical takeoff and landing aircraft," *J. Power Sources*, vol. 620, Nov. 2024, Art. no. 235188.
[17] P. Pillai, J. Nguyen, and B. Balasingam, "Performance analysis of empirical open-circuit voltage modeling in lithium-ion batteries, part-2: Data collection procedure," *IEEE Trans. Transp. Electrific.*, vol. 11, no. 1, pp. 153–162, Feb. 2025.
[18] R. Guo and W. Shen, "An enhanced multi-constraint state of power estimation algorithm for lithium-ion batteries in electric vehicles," *J. Energy Storage*, vol. 50, Jun. 2022, Art. no. 104628.